An apparatus for measuring combined shear-tensile loading in fibrous tissues *ex vivo*

Jonathon L. Blank
Department of Mechanical Engineering, University of Wisconsin-Madison, Madison, WI
1513 University Avenue Room 3046, Madison, WI 53706
jonathon.blank@pennmedicine.upenn.edu

Joshua D. Roth
Department of Mechanical Engineering, University of Wisconsin-Madison, Madison, WI
Department of Orthopedics and Rehabilitation, University of Wisconsin-Madison, Madison, WI
1111 Highland Avenue Room 5037, Madison, WI 53705
roth@ortho.wisc.edu

ABSTRACT

Soft tissues such as tendon and ligament undergo a combination of shear and tensile loading in vivo due to their boundary conditions at muscle and/or bone. Current experimental protocols are limited to either pure tensile loading, biaxial loading, or simple shear, and thus may not fully characterize the mechanics of these tissues under physiological loading scenarios. Our objective was to create an experimental protocol to determine the shear modulus of fibrous tissues at different tensile loads. We assembled a four-actuator experimental system that facilitated shear deformation to be superimposed on a tissue subjected to an axial preload. We measured shear modulus in axially loaded electrospun nanofiber scaffolds with either randomly-oriented or aligned fibers. We found that shear modulus in the nanofiber phantoms was shear-strain stiffening and dependent on both the axial load ($p < 0.001$) and fiber alignment ($p < 0.001$) of the scaffold. The proposed system can enhance our understanding of microstructure and functional mechanics in soft tissues, while also providing a platform to investigate the behavior of electrospun scaffolds for tissue regeneration. Our experimental protocol for determining loaded shear modulus would be further useful as a method to gauge tissue mechanics under loading conditions that are more representative of physiological loads applied to tendon and ligament.

1. Introduction

Tendons and ligaments are musculoskeletal soft tissues that connect muscle to bone and bone to bone, respectively. Tendons transmit forces generated by individual and/or groups of muscles to enable joint motion. Ligaments serve to passively guide joint motion across a broad range of relative bone rotations and translations to fulfill their anatomical function (Wilson, Feikes, and O'Connor 1998). Due to these unique boundary conditions, the physiological loading of these tissues is highly complex, resulting in nonuniform deformations due to both axial and shear loads (Gardiner and Weiss 2003; Willinger et al. 2020). The microstructure of these tissues directly affects how they respond to complex physiological loading (Lake et al. 2010; Blank et al. 2021; Blank, Thelen, and Roth 2023), where tendons have highly aligned fibers, and ligaments exhibit a more distributed fiber alignment (Amis 1998; Provenzano and Vanderby 2006). The health state of the tissue also can substantially alter microstructure and mechanics, such as in tendinopathy (Arya and Kulig 2010) and following injury or repair (Freedman et al. 2016). Thus, understanding the microstructure-function relationships of musculoskeletal soft tissues like tendons and ligaments requires mechanical tests that induce complex loading and consider fiber alignment as a feature that may alter their mechanics.

Despite the complex loading in vivo, benchtop methods for assessing the mechanics of musculoskeletal tissues have been mostly limited to tensile testing, and in some cases shear or biaxial testing (Claeson and Barocas 2017; Tan et al. 2016) of tissue sections or representative scaffolds (Weiss, Gardiner, and Bonifasi-Lista 2002; Gardiner and Weiss 2001; Driscoll et al. 2011). These techniques have enabled a better understanding of the capacity for healthy tissues to transmit load and their mechanics within these simple loading paradigms. Other studies have characterized the combined mechanics within a tissue during either tension or shear, such as interfibrillar shear strain (Szczesny and Elliott 2014; Muench, Thelen, and Henak 2020) and stress (Szczesny et al. 2015) within a tendon

fascicle during tension, or the distribution of stress and tensile forces within a tissue during shear. However, the mechanics resulting from combined shear-tensile loading remains unelucidated.

Accordingly, the objectives of this study were to (1) develop a novel loading paradigm for determining the axially preloaded shear modulus of fibrous soft tissues, and (2) characterize differences in shear behavior in isotropic and anisotropic fibrous tissues using this loading paradigm. We hypothesized that shear modulus in the isotropic scaffold would be higher than the anisotropic scaffold due to unaligned fibers resisting shear (Blank et al. 2021). To accomplish these objectives, we constructed a fixture capable of applying combined shear-tensile loading. We fabricated isotropic and anisotropic tissue scaffolds, which we expected would have different shear responses, and characterized their tangential shear modulus in the axially preloaded state.

2. Methods

2.1 Shear-Tensile Loading Paradigm

To compute the loaded shear modulus, we consider a sample undergoing deformation at four different locations (Fig. 1). The two top grips attached to the sample are translated to load the sample in axial tension. Next, the two grips from one side are translated to load the middle of the sample in shear while maintaining the initial axial tension. We consider the sample to be symmetric in its force balance about the centerline of the structure, and thus, can resolve the shear force acting on the longitudinal cross-section along the centerline from the force balance of one side (Fig. 1c). The average shear stress can be resolved as the shear force over the cross-sectional area of the section. The shear strain applied can be computed using the width of the shear region between the left and right grips. These two measures represent the effective average shear stress and the maximum shear strain applied to the center region of the sample.

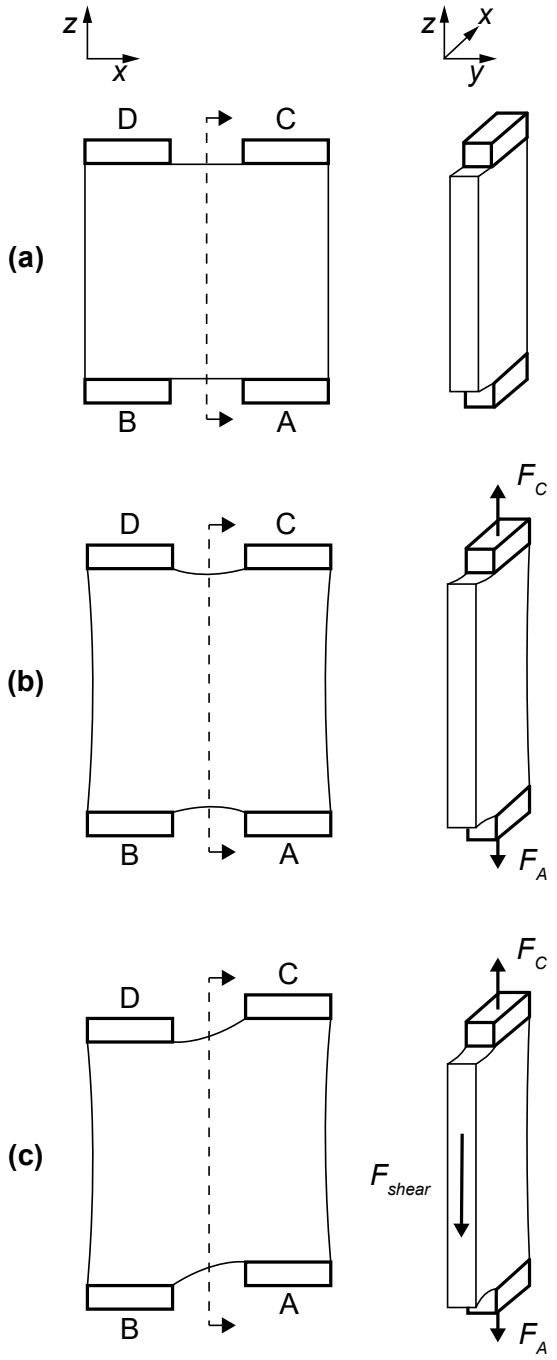

Figure 1: (a) A tissue section subject to a combination of **(b)** tension (in the *z*-direction, where $F_c = -F_A$) and **(c)** shear (in the *xz*-plane). The shear force can be resolved as $F_{shear} = F_c - F_A$.

2.2. Fixture Design

We designed an experimental system that is capable of loading a tissue section according to the paradigm outlined in Section 2.1. Our fixture consisted of four motor-driven linear actuators (Kollmorgen EN60034, < 20 µm backlash, 2 top, 2 bottom) that were each instrumented with a submersible load cell (Futek LSB210). Each load cell was attached to a 3D-printed grip lined with sandpaper to minimize the chance that the specimen slips within the grip. The entire instrumented grip system was placed in an acrylic bath with a window for backlit optical measures of strain (Raghupathy et al. 2011) or fiber alignment (York et al. 2014).

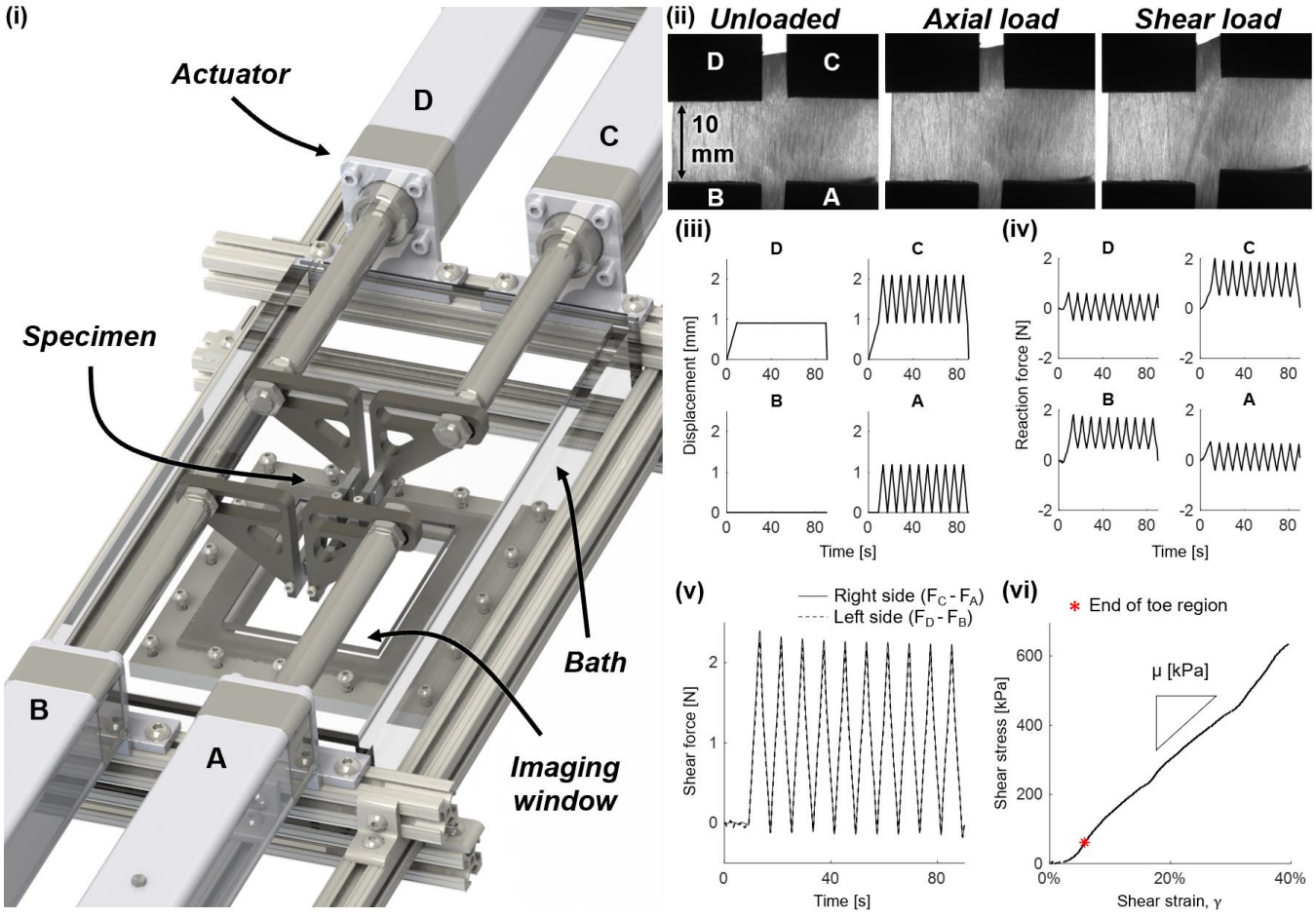

Figure 2: (i) We designed and fabricated a fixture capable of loading a soft tissue sample in combined shear and tension. The fixture featured four actuators (A-D), a bath, and a transparent imaging window through which backlit videos could be recorded. **(ii)** Specimens seen in polarized light images were loaded first in tension and then in shear. **(iii-iv)** The plots show that the four actuators moved independently to load the soft tissue to an axial strain of 0-9% and a shear strain of 0-40%. **(v)** Plot shows that the shear force was computed on both sides of the specimen and found to be equal, indicating force balance across the tissue width. **(vi)** Plot shows how we computed the shear modulus in the linear region of the shear stress-shear strain curve.

2.3. Implementation in Fibrous Tissues

2.3.1. Specimen preparation

We prepared poly-ε-caprolactone (PCL) scaffolds via electrospinning (Li et al. 2002). We dissolved PCL in a 7:1 mixture of chloroform (TCM) and *N*,*N*-dimethylformamyde (DMF) to achieve a 0.12 g/mL PCL solution. We chose TCM as a solvent because it was capable of producing fibers that were a similar diameter as observed in tendon and ligament (1-20 um) and added DMF to increase the dielectric potential of our mixture. The polymer solution was driven through an 18-gauge needle at 1.2 mL/hr with a 16kV potential through a distance of 10 cm. A rotating, circular drum with a diameter of 11.75 cm was placed in the polymer jet path (Fig. S1). We controlled rotation speed to generate anisotropic fiber scaffolds with fiber alignments that spanned a near-isotropic alignment (linear velocity = 0.2 m/s) to highly aligned fibers (linear velocity = 14 m/s) (Li et al. 2007; Barber et al. 2013) (Fig. S1).

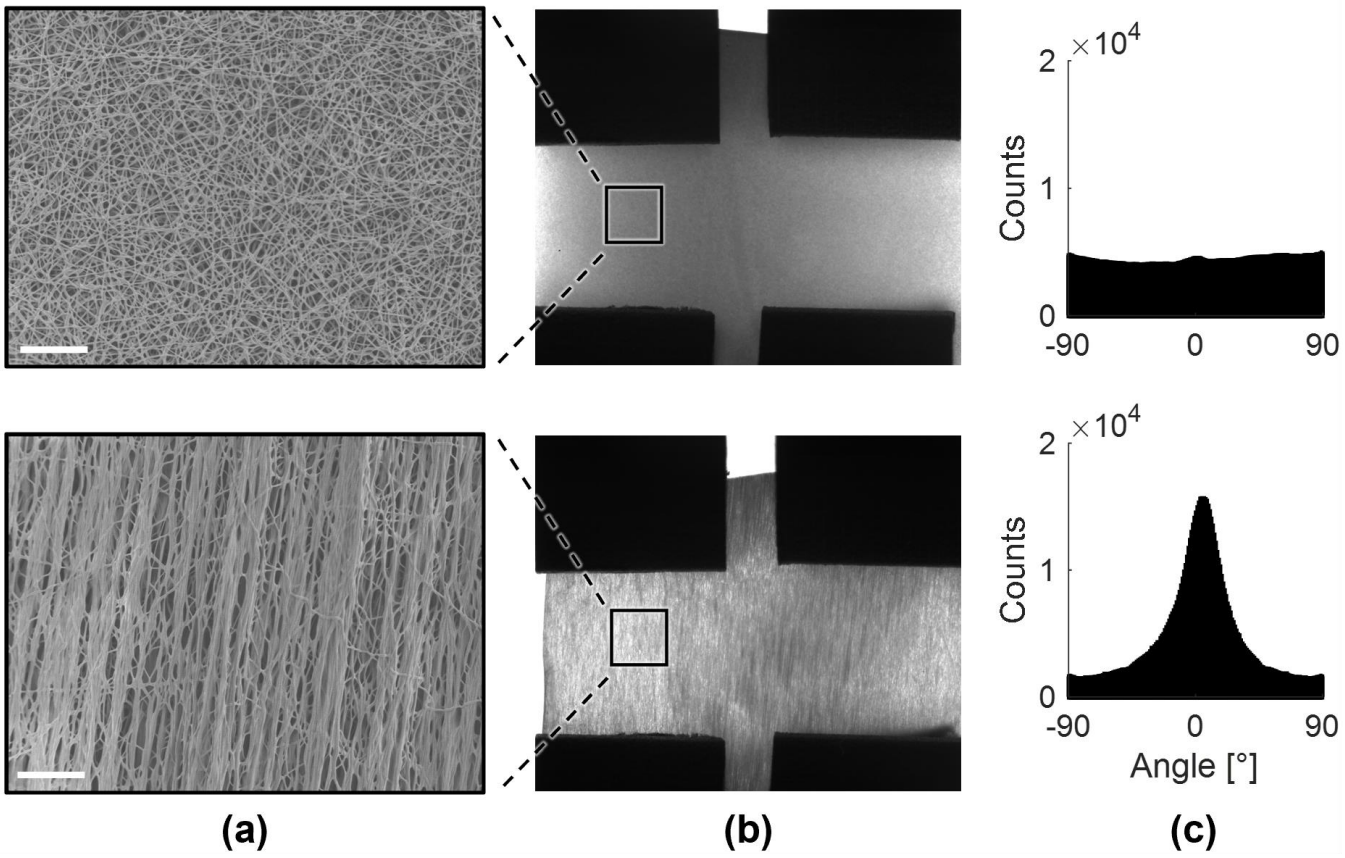

Figure 3: (a-b) We created two electrospun scaffolds, one with isotropic fibers (bottom electron microscope and polarized light images) and one with anisotropic fibers (top electron microscope and polarized light images). Scale bars represent 100 µm. **(c)** We characterized the fiber angle of the scaffold when loaded into the grips of the testing fixture based on the polarized light images (b). The isotropic fiber scaffold had a near-uniform distribution of fibers (top histogram), while the anisotropic scaffold had a high concentration of fibers oriented along the loading direction (bottom histogram).

2.3.2. Imaging

We imaged all electrospun scaffolds to verify fiber alignment. Representative sections from each scaffold were sputter-coated with gold and mounted in a scanning electron microscope (SEM) (Zeiss Gemini 300). Three images of the surface of each scaffold were recorded at 200x (1024 x 768 pixels).

To determine fiber alignment, we applied a 5x5 Prewitt operator (Kekre and Gharge 2010) to the greyscale intensity values of each SEM image. We then determined the orientation of each pixel group. Angle values were then binned and centered at 0° to confirm the isotropy of the scaffold. The fiber alignment was assumed to be constant across all specimens from a single scaffold.

2.3.3. Mechanical testing

We mounted n=5 specimens per fiber alignment level between sandpaper grips on a custom axial-shear dynamic testing fixture (Fig. 2). The four motor-driven linear actuators (<20 μm backlash) loaded the specimen both in axial tension and shear (Fig. 2). These actuators were controlled using a commercially available software in LabVIEW (simVITRO, Cleveland Clinic). Prior to testing, we recorded the thickness of each specimen using three repeated caliper measurements along the length of the structure. The width was computed as the average of these measurements. We preloaded each specimen to between 0.05 and 0.1 N tension on either side. After preloading, we loaded each specimen in shear with a sawtooth displacement profile from 0-40% shear strain at a rate of 10%/s for 10 cycles. We then loaded specimens to axial strains of 3, 6, and 9% at a rate of 1%/s. At each axial strain, we applied the same sawtooth shear displacement profile.

2.3.4. Shear modulus computation

We measured shear modulus during the last cycle to minimize viscoelastic effects. If viscoelasticity (i.e., stress relaxation following the axial prestrain) was still present, the stress-relaxation component of the axial loading was fit using a first-order exponential and subtracted from the overall axial-shear load to obtain an approximation of the elastic response (Fig. S2). We determined the linear

region of the shear stress response using an exponential-linear optimization function (Tanaka et al. 2011). The shear modulus was then computed as the slope of a linear fit to the linear region.

2.4. Statistical Analyses

We assessed the shear modulus (μ) at each axial prestrain level (ε). We compared the shear moduli of the isotropic and anisotropic scaffolds at each level of axial prestrain using a two-factor analysis of variance (ANOVAs) with post-hoc Tukey tests. The first factor was fiber alignment (2 levels: isotropic and anisotropic), and the second factor was axial prestrain (4 levels: 0%, 3%, 6%, 9%). Because our data violated the sphericity assumption ($\varepsilon_{shpericity} = 0.37$), we used Greenhouse-Geisser corrections to conservatively estimate significance of differences across axial prestrain and fiber alignment. For all analyses, we set significance at $\alpha = 0.05$.

3. Results

The shear moduli of both the isotropic and anisotropic scaffolds increased monotonically with increasing axial prestrain (Table 1). We measured an unloaded shear modulus of 1148 ± 174 kPa in the isotropic scaffold, which was higher than the unloaded shear modulus of 289 ± 97 kPa in the anisotropic scaffold ($p < 0.001$). The shear modulus of the isotropic scaffold was higher than the anisotropic scaffold at all other levels of axial prestrain ($p < 0.001$).

Table 1: Shear modulus (in kPa) measured at each axial prestrain level for n = 5 isotropic and n = 5 anisotropic electrospun scaffolds. The right column indicates the p-value of the post-hoc Tukey tests.

	Shear modulus [kPa]		
Prestrain	**Isotropic**	**Anisotropic**	**p-value**
0%	1148 ± 174	289 ± 97	< 0.001
3%	1269 ± 225	366 ± 122	< 0.001

6%	1397 ± 265	441 ± 152	< 0.001
9%	1547 ± 2710	498 ± 150	< 0.001

The shear modulus of the isotropic scaffold was consistently greater than the shear modulus of the anisotropic scaffold (Fig. 4). For both scaffold types, shear modulus was dependent on the axial prestrain ($p < 0.001$). We also detected a significant interaction between the degree of anisotropy of the scaffolds and axial prestrain on tangential shear modulus ($p = 0.016$).

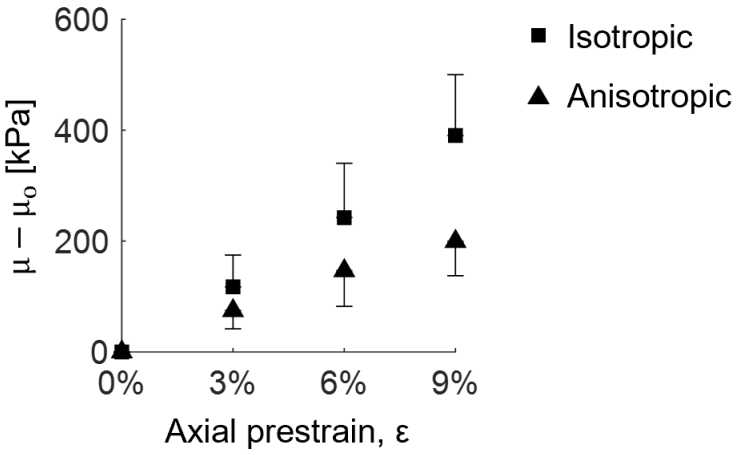

Figure 4: Increase in shear modulus across axial prestrain levels in the isotropic and anisotropic electrospun scaffolds relative to the unloaded shear moduli. Tangential shear modulus in both scaffolds increased monotonically with increasing axial prestrain. Points represent the mean increases, and error bars represent the standard deviation of the increases.

4. Discussion

The objectives of this study were to (1) develop a novel loading paradigm for determining the axially preloaded shear modulus of fibrous soft tissues, and (2) characterize differences in shear behavior in isotropic and anisotropic fibrous tissue scaffolds using this loading paradigm. Our first key contribution was that we successfully constructed a benchtop testing system capable of producing

combined shear-tensile loading in a tissue sample. Using this loading paradigm, we presented a method to compute the tangential shear modulus of the tissue in the axially preloaded state. Our second key contribution was to demonstrate that this method was sufficiently sensitive to detect changes in the tangential shear modulus across both axial prestrain levels and in tissue surrogates with different fiber alignments.

Concerning our first objective, we constructed a fixture capable of resolving the shear modulus of a soft tissue section under an axial prestrain (Figs. 1 and 2). Previously, shear testing in musculoskeletal soft tissues was limited to either simple (Bonifasi-Lista et al. 2005; Weiss, Gardiner, and Bonifasi-Lista 2002; Gardiner and Weiss 2001) or interfibrillar (Szczesny et al. 2015; Szczesny and Elliott 2014; Muench, Thelen, and Henak 2020) shear. Thus, to our knowledge, this is the first implementation of a benchtop technique to determine the pretensioned shear modulus of a fibrous soft tissue section. This system is adaptable to test a range of tissue scales from thin sections required when performing simultaneous polarized light imaging to complete ligaments/tendons. Only the capacity of the load cells would need to change between these tissue scales. Additionally, the linear actuators we selected are capable of much greater loads than necessary for most applications of ligament-tendon testing. Thus, if building a system from scratch with this particular loading paradigm in mind, then different actuators could be used following the design and loading paradigm developed in this study.

Concerning our second objective, we found that our fixture was capable of resolving the axially prestrained shear modulus and was sensitive enough to detect changes in shear modulus due to both fiber alignment ($p < 0.001$) and axial prestrain ($p < 0.001$) (Table 1 and Fig. 4). This finding has important implications to both our fundamental understanding of the structure-function relationship of musculoskeletal soft tissues and our understanding about how to design electrospun nanofiber scaffolds to best replicate the mechanical environment of biological tissues. Regarding the first implication, these

findings demonstrate how tissues with more anisotropic fiber alignments (e.g., ligaments) become stiffer in shear as the tissue is axially strained, which likely enhances load transfer across a wide range of joint configurations (Provenzano and Vanderby 2006; Lake et al. 2010). We also found that more highly aligned scaffolds had a smaller increase in shear modulus across axial prestrain levels. This finding may be informative for the function of tendons, which have relatively more highly aligned fibers than ligaments due to transmitting primarily axial loads. However, tendons also feature a bony insertion, areas of compression, and an interface with an in-series muscle that may contribute to anisotropic material properties relevant to both tension and shear (Thomopoulos et al. 2003; Wheatley et al. 2023; Shan et al. 2021; Lake et al. 2010). Regarding the second implication, we characterized shear mechanics in electrospun scaffolds, which are required to undergo unique loading paradigms to replicate the musculoskeletal loading environment when used for tissue engineering/regeneration (Brennan et al. 2018). To this point, scaffolds are often designed to replicate the alignment, and thus mechanics of tissues (Nerurkar, Elliott, and Mauck 2007; Li et al. 2007). Scaffolds can also be used to model different tissues or different tissue regions (Xie et al. 2010). Because shear mechanics, in particular, are sensitive to alignment or orientation of fibers (Driscoll et al. 2011), the pretensioned shear modulus may be a consideration for these scaffolds to better replicate the native loading environment of their target tissue.

Our mechanical testing procedure has a few limitations to consider when interpreting results. First, it is likely that the current protocol is sensitive to viscoelastic effects despite preconditioning specimens both axially and in shear. At sequential axial prestrains, it is likely that the tissue is stress relaxing and stretching over time. Thus, the axially prestrained shear moduli may be underestimated due to a lower overall axial tension over time. The axial prestrain order should thus be randomized in future tests to further eliminate the influence of viscoelastic effects in test results and to reduce the effect of systematic effects. A force or hybrid-controlled implementation may also better mitigate viscoelastic

effects due to stress relaxation. Second, our results are likely sensitive to the horizontal spacing of the four grips (*x*-direction, Fig. 1). We used preliminary finite element models to choose the horizontal spacing of our grips (3 mm) based on comparisons to controlled single-element predictions of loaded shear, but it is possible that a wider spacing may better reflect the physiological mechanics of different tissue types, and thus grip spacing should be considered for each application of this technique. Third, while not a limitation of the technique overall, we chose to examine scaffolds with two different fiber alignments that roughly represent a range of alignments encountered in musculoskeletal tissues. More studies are required to determine the sensitivity of this technique to more subtle variations in fiber alignment.

In conclusion, we presented a novel technique for resolving the axially preloaded shear modulus. This technique should be considered to enhance ongoing analysis of structure, function, and mechanics in musculoskeletal soft tissues or electrospun scaffolds for tissue regeneration.

Acknowledgments

We gratefully acknowledge Dr. Darryl Thelen for his technical insight into devising a combined shear-tensile loading paradigm. We thank Dr. Wan-Ju Li for his assistance in fabricating nanofiber scaffolds. We thank Dr. Julie Morasch and the University of Wisconsin-Madison Nanoscale Imaging and Analysis Center (NIAC) for their assistance in obtaining scanning electron microscope images. The authors would also like to acknowledge the simVITRO team for their support with software implementation of our loading paradigm.

Funding

This material is based upon work supported by the National Science Foundation Graduate Research Fellowship Program under Grant No. DGE-1747503. Any opinions, findings, and conclusions or recommendations expressed in this material are those of the author(s) and do not necessarily reflect the views of the National Science Foundation.

Funding for materials in this project came from Dr. Roth's start-up funds through the UW-Madison Department of Orthopedics and Rehabilitation.

References

Amis, Andrew A. 1998. "Biomechanics of Bone, Tendon, and Ligament." In *Sciences Basic to Orthopaedics,* 222–39.

Arya, Shruti, and Kornelia Kulig. 2010. "Tendinopathy Alters Mechanical and Material Properties of the Achilles Tendon." *Journal of Applied Physiology* 108 (3): 670–75. https://doi.org/10.1152/japplphysiol.00259.2009.

Barber, John G., Andrew M. Handorf, Tyler J. Allee, and Wan Ju Li. 2013. "Braided Nanofibrous Scaffold for Tendon and Ligament Tissue Engineering." *Tissue Engineering - Part A* 19 (11–12): 1265–74. https://doi.org/10.1089/ten.tea.2010.0538.

Blank, Jonathon L., Darryl G. Thelen, Matthew S. Allen, and Joshua D. Roth. 2021. "Sensitivity of the Shear Wave Speed-Stress Relationship to Soft Tissue Material Properties and Fiber Alignment." *Journal of the Mechanical Behavior of Biomedical Materials* 125 (November 2021): 104964. https://doi.org/10.1016/j.jmbbm.2021.104964.

Blank, Jonathon L., Darryl G. Thelen, and Joshua D. Roth. 2023. "Regional Shear Wave Speeds Track Regional Axial Stress in Nonuniformly Loaded Fibrous Soft Tissues." *EngrXiv*. https://doi.org/10.31224/2923.

Bonifasi-Lista, Carlos, Spencer P. Lake, Michael S. Small, and Jeffrey A. Weiss. 2005. “Viscoelastic Properties of the Human Medial Collateral Ligament under Longitudinal, Transverse and Shear Loading.” *Journal of Orthopaedic Research* 23 (1): 67–76. https://doi.org/10.1016/j.orthres.2004.06.002.

Brennan, David A., Adriano A. Conte, Gregory Kanski, Stefan Turkula, Xiao Hu, Matthew T. Kleiner, and Vince Beachley. 2018. “Mechanical Considerations for Electrospun Nanofibers in Tendon and Ligament Repair.” *Advanced Healthcare Materials* 7 (12): 1–31. https://doi.org/10.1002/adhm.201701277.

Claeson, Amy A., and Victor H. Barocas. 2017. “Planar Biaxial Extension of the Lumbar Facet Capsular Ligament Reveals Significant In-Plane Shear Forces.” *Journal of the Mechanical Behavior of Biomedical Materials* 65: 127–36. https://doi.org/10.1016/j.jmbbm.2016.08.019.

Driscoll, Tristan P., Nandan L. Nerurkar, Nathan T. Jacobs, Dawn M. Elliott, and Robert L. Mauck. 2011. “Fiber Angle and Aspect Ratio Influence the Shear Mechanics of Oriented Electrospun Nanofibrous Scaffolds.” *Journal of the Mechanical Behavior of Biomedical Materials* 4 (8): 1627–36. https://doi.org/10.1016/j.jmbbm.2011.03.022.

Freedman, Benjamin R., Joshua A. Gordon, Pankti R. Bhatt, Adam M. Pardes, Stephen J. Thomas, Joseph J. Sarver, Corinne N. Riggin, et al. 2016. “Nonsurgical Treatment and Early Return to Activity Leads to Improved Achilles Tendon Fatigue Mechanics and Functional Outcomes during Early Healing in an Animal Model.” *Journal of Orthopaedic Research* 34 (12): 2172–80. https://doi.org/10.1002/jor.23253.

Gardiner, J. C., and J. A. Weiss. 2001. “Simple Shear Testing of Parallel-Fibered Planar Soft Tissues.” *Journal of Biomechanical Engineering* 123 (2): 170–75. https://doi.org/10.1115/1.1351891.

Gardiner, J C, and J A Weiss. 2003. “Subject-Specific Finite Element Models Can Predict Strain in the

Human Medial Collateral Ligament." *Journal of Orthopaedic Research* 21: 1098–1106. https://doi.org/10.1016/S0736-0266(03)00113-X.

Kekre, Hemant B, and Saylee Gharge. 2010. "Image Segmentation Using Extended Edge Operator for Mammographic Images." *International Journal on Computer Science and Engineering*, no. June 2014.

Lake, Spencer P., Kristin S. Miller, Dawn M. Elliott, and Louis J. Soslowsky. 2010. "Tensile Properties and Fiber Alignment of Human Supraspinatus Tendon in the Transverse Direction Demonstrate Inhomogeneity, Nonlinearity, and Regional Isotropy." *Journal of Biomechanics* 43 (4): 727–32. https://doi.org/10.1016/j.jbiomech.2009.10.017.

Li, Wan Ju, Cato T. Laurencin, Edward J. Caterson, Rocky S. Tuan, and Frank K. Ko. 2002. "Electrospun Nanofibrous Structure: A Novel Scaffold for Tissue Engineering." *Journal of Biomedical Materials Research* 60 (4): 613–21. https://doi.org/10.1002/jbm.10167.

Li, Wan Ju, Robert L. Mauck, James A. Cooper, Xiaoning Yuan, and Rocky S. Tuan. 2007. "Engineering Controllable Anisotropy in Electrospun Biodegradable Nanofibrous Scaffolds for Musculoskeletal Tissue Engineering." *Journal of Biomechanics* 40 (8): 1686–93. https://doi.org/10.1016/j.jbiomech.2006.09.004.

Muench, Jared R., Darryl G. Thelen, and Corinne R. Henak. 2020. "Interfibrillar Shear Behavior Is Altered in Aging Tendon Fascicles." *Biomechanics and Modeling in Mechanobiology* 19 (3): 841–49. https://doi.org/10.1007/s10237-019-01251-0.

Nerurkar, NL, DM Elliott, and RL Mauck. 2007. "Mechanics of Oriented Electrospun Nanofibrous Scaffolds for Annulus Fibrosus Tissue Engineering Nandan." *Journal of Orthopaedic Research* 25 (August): 1018–28. https://doi.org/10.1002/jor.

Provenzano, Paolo P., and Ray Vanderby. 2006. "Collagen Fibril Morphology and Organization:

Implications for Force Transmission in Ligament and Tendon." *Matrix Biology* 25 (2): 71–84. https://doi.org/10.1016/j.matbio.2005.09.005.

Raghupathy, Ramesh, Colleen Witzenburg, Spencer P. Lake, Edward A. Sander, and Victor H. Barocas. 2011. "Identification of Regional Mechanical Anisotropy in Soft Tissue Analogs." *Journal of Biomechanical Engineering* 133 (9). https://doi.org/10.1115/1.4005170.

Shan, Xiyao, Shun Otsuka, Le Li, and Yasuo Kawakami. 2021. "Inhomogeneous and Anisotropic Mechanical Properties of the Triceps Surae Muscles and Aponeuroses in Vivo during Submaximal Muscle Contraction." *Journal of Biomechanics* 121. https://doi.org/10.1016/j.jbiomech.2021.110396.

Szczesny, Spencer E., Jeffrey L. Caplan, Pal Pedersen, and Dawn M. Elliott. 2015. "Quantification of Interfibrillar Shear Stress in Aligned Soft Collagenous Tissues via Notch Tension Testing." *Scientific Reports* 5 (December 2014): 1–9. https://doi.org/10.1038/srep14649.

Szczesny, Spencer E., and Dawn M. Elliott. 2014. "Interfibrillar Shear Stress Is the Loading Mechanism of Collagen Fibrils in Tendon." *Acta Biomaterialia* 10 (6): 2582–90. https://doi.org/10.1016/j.actbio.2014.01.032.

Tan, Ting, Nathan M. Cholewa, Scott W. Case, and Raffaella De Vita. 2016. "Micro-Structural and Biaxial Creep Properties of the Swine Uterosacral–Cardinal Ligament Complex." *Annals of Biomedical Engineering* 44 (11): 3225–37. https://doi.org/10.1007/s10439-016-1661-z.

Tanaka, Martin L., Charles A. Weisenbach, Mark Carl Miller, and Laurel Kuxhaus. 2011. "A Continuous Method to Compute Model Parameters for Soft Biological Materials." *Journal of Biomechanical Engineering* 133 (7): 1–7. https://doi.org/10.1115/1.4004412.

Thomopoulos, Stavros, Gerald R. Williams, Jonathan A. Gimbel, Michele Favata, and Louis J. Soslowsky. 2003. "Variation of Biomechanical, Structural, and Compositional Properties along the

Tendon to Bone Insertion Site." *Journal of Orthopaedic Research* 21 (3): 413–19. https://doi.org/10.1016/S0736-0266(03)0057-3.

Weiss, Jeffrey A., John C. Gardiner, and Carlos Bonifasi-Lista. 2002. "Ligament Material Behavior Is Nonlinear, Viscoelastic and Rate-Independent under Shear Loading." *Journal of Biomechanics* 35 (7): 943–50. https://doi.org/10.1016/S0021-9290(02)00041-6.

Wheatley, Benjamin B., Olivia L. Dyer, Emily E. Tully, and Mark A. Seeley. 2023. "Aponeurosis Structure-Function Properties: Evidence of Heterogeneity and Implications for Muscle Function." *Acta Biomaterialia* 168: 298–308. https://doi.org/10.1016/j.actbio.2023.06.035.

Willinger, Lukas, Shun Shinohara, Kiron K. Athwal, Simon Ball, Andy Williams, and Andrew A. Amis. 2020. "Length-Change Patterns of the Medial Collateral Ligament and Posterior Oblique Ligament in Relation to Their Function and Surgery." *Knee Surgery, Sports Traumatology, Arthroscopy* 28 (12): 3720–32. https://doi.org/10.1007/s00167-020-06050-0.

Wilson, D. R., J. D. Feikes, and J. J. O'Connor. 1998. "Ligaments and Articular Contact Guide Passive Knee Flexion." *Journal of Biomechanics* 31 (12): 1127–36. https://doi.org/10.1016/S0021-9290(98)00119-5.

Xie, Jingwei, Xiaoran Li, Justin Lipner, Cionne N. Manning, Annie G. Schwartz, Stavros Thomopoulos, and Younan Xia. 2010. "'Aligned-to-Random' Nanofiber Scaffolds for Mimicking the Structure of the Tendon-to-Bone Insertion Site." *Nanoscale* 2 (6): 923–26. https://doi.org/10.1039/c0nr00192a.

York, Timothy, Lindsey Kahan, Spencer P. Lake, and Viktor Gruev. 2014. "Real-Time High-Resolution Measurement of Collagen Alignment in Dynamically Loaded Soft Tissue." *Journal of Biomedical Optics* 19 (06): 1. https://doi.org/10.1117/1.jbo.19.6.066011.

SUPPLEMENTARY MATERIALS

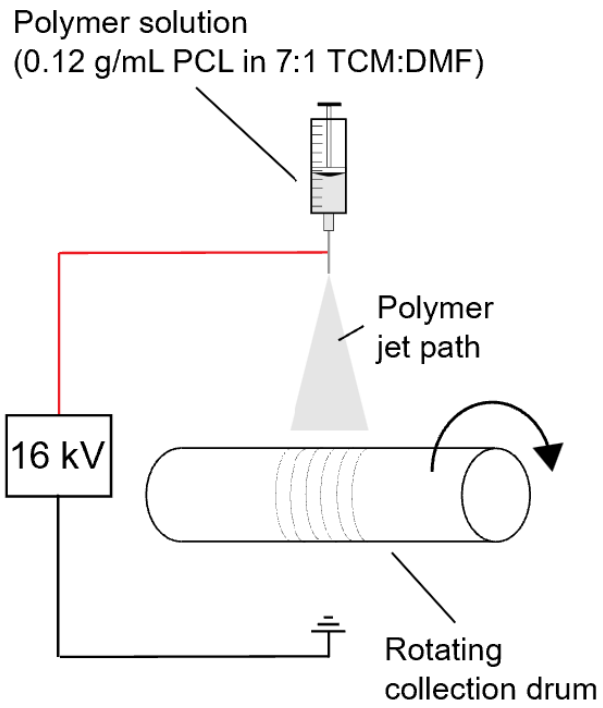

Figure S1: (a-b) We created two electrospun scaffolds, one with isotropic fibers and one with more aniotropic fibers. **(c)** We characterized the fiber angle of the scaffold when loaded into the grips of the testing fixture. **(d)** Fiber angles were then fit with a von Mises function (k_f = whole number) to inform our finite element model.

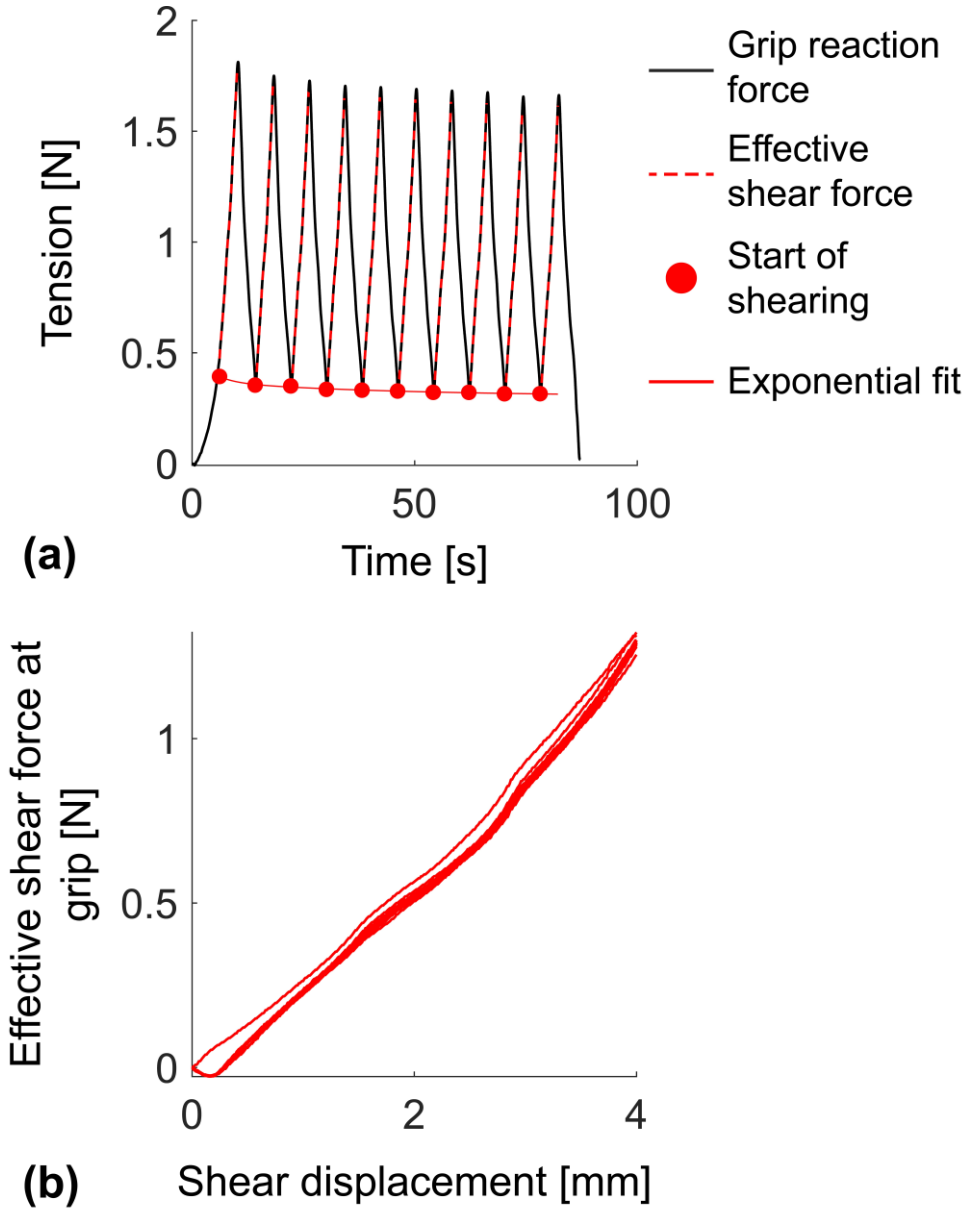

376

377 **Figure S2: (a)** We fit an exponential curve to the stress relaxation response of each grip to approximate

378 the shear forces at the grip. **(b)** The effective shear force at the grip (taken as the exponential fit from (a)

379 subtracted from the total grip reaction force) during shearing was consistent across the testing period.

380 We used the last cycle only (all ten cycles shown) to minimize viscoelastic effects.

381